Journal of Solid State Chemistry 182 (2009) 2806–2814

Contents lists available at ScienceDirect

Journal of Solid State Chemistry

journal homepage: www.elsevier.com/locate/jssc

Compositional control of electrical transport properties in the new series of defect thiospinels, $Ga_{1-x}Ge_xV_4S_{8-\delta}$ $(0 \le x \le 1)$

Iwona Szkoda [a], Paz Vaqueiro [a], Andrew McDowall [a], Anthony V. Powell [a,*], Clemens Ritter [b]

[a] Department of Chemistry, Heriot-Watt University, Edinburgh EH14 4AS, UK
[b] Institut Max von Laue—Paul Langevin, F-38042 Grenoble, France

ARTICLE INFO

Article history:
Received 15 May 2009
Received in revised form
17 July 2009
Accepted 24 July 2009
Available online 3 August 2009

Keywords:
Crystal structure
Transport properties
Neutron diffraction
Magnetic properties
Chalcogenides

ABSTRACT

A new series of non-stoichiometric sulfides $Ga_{1-x}Ge_xV_4S_{8-\delta}$ $(0 \le x \le 1;\ \delta \le 0.23)$ has been synthesized at high temperatures by heating stoichiometric mixtures of the elements in sealed quartz tubes. The samples have been characterized by powder X-ray diffraction, SQUID magnetometry and electrical transport-property measurements. Structural analysis reveals that a solid solution is formed throughout this composition range, whilst thermogravimetric data reveal sulfur deficiency of up to 2.9% in the quaternary phases. Magnetic measurements suggest that the ferromagnetic behavior of the end-member phase GaV_4S_8 is retained at $x \le 0.7$; samples in this composition region showing a marked increase in magnetization at low temperatures. By contrast $Ga_{0.25}Ge_{0.75}V_4S_{8-\delta}$ appears to undergo antiferromagnetic ordering at ca. 15 K. All materials with $x \ne 1$ are n-type semiconductors whose resistivity falls by almost six orders of magnitude with decreasing Ga content, whilst the end-member phase $GeV_4S_{8-\delta}$ is a p-type semiconductor. The results demonstrate that the physical properties are determined principally by the degree of electron filling of narrow-band states arising from intracluster V–V interactions.

1. Introduction

Many compounds of general formula AB_2S_4 adopt a spinel-type structure in which *A* and *B* cations are distributed over tetrahedral and octahedral sites within a cubic-close packed array of anions. In the normal thiospinel structure, *A* cations exclusively occupy $\frac{1}{8}$ of the tetrahedral sites with *B* cations occupying 50% of the octahedral sites in an ordered fashion [1]. Whilst cation deficiency is much less common amongst the thiospinels than in nickel arsenide type phases [2,3], there exists a small family of defective spinel-like materials, in which *A*-site cation deficiency gives rise to a superstructure. These materials of general formula $A_{0.5}B_2S_4$ $(\equiv AB_4S_8)$ exhibit *A*-site vacancy ordering leading to a structure which consists of heterocubane-like $B_4S_4^{n+}$ clusters and AS_4^{n-} tetrahedra. These structural units adopt a rocksalt-like arrangement in the cubic unit cell observed at room temperature (Fig. 1). Ordering of the *A* cations over the tetrahedral sites lowers the $Fd\bar{3}m$ symmetry of the ideal spinel structure to $F\bar{4}3m$, while displacement of the B-cations results in B_4 clusters with short *B*–*B* distances (ca. 2.8 Å).

Following the first report [4] of the ferromagnetic semiconducting spinels, $GaMo_4X_8$ $(X = S, Se)$, materials of general formula AB_4S_8 have been prepared for $A =$ Ga, Ge, Al and $B =$ Mo, V, Nb [5–7]. Further flexibility is provided by the ability of the A-site to accommodate additional cations in materials such as $GaM_xMo_4S_8$ $(M =$ C, Si, Ge) [8] and to tolerate appreciable levels of cation deficiency as observed in $Ga_{0.87}Ti_4S_8$ [9]. The effects of cation substitution at the *A*-site have been explored in $Ga_{1-x}Zn_xV_4S_8$ [10]. In addition to the mixed *B*-site materials $M[Mo_2Re_2]S_8$ $(M =$ Mg, Fe, Co, Ni, Cu, Zn) [11], the effects of chemical substitution at the *B*-site have been investigated through preparation of the non-stoichiometric series $Ga_xV_{4-y}Cr_yS_8$ [12] and $GaV_{4-x}Mo_xS_8$ [13].

The defect thiospinels are Mott insulators in which electrical conduction occurs by inter-cluster hopping of electrons [14] over relatively large distances of 4 Å. It has been proposed that GaV_4S_8 behaves as a Fermi glass at low temperatures [15]. Unpaired electrons are thus effectively localized on the cluster with the consequence that at low temperatures, the materials may exhibit cooperative magnetism arising from exchange interactions between *B* cations. For example, the ternary phases GaV_4S_8 [16] and $GaMo_4S_8$ [4] exhibit weak ferromagnetism below $T_C = 10$ and 16 K respectively. Both ternary phases also exhibit a second anomaly in magnetic susceptibility data at ca. 40 K, which is associated with a structural transition involving a rhombohedral distortion. We have recently shown [13] using high-resolution neutron and synchrotron X-ray diffraction that the phase transition in each case is incomplete leading to the coexistence of rhombohedral and cubic phases at low temperature.

* Corresponding author. Fax: +44 131 451 3180.
E-mail address: a.v.powell@hw.ac.uk (A.V. Powell).

0022-4596/$ - see front matter © 2009 Elsevier Inc. All rights reserved.
doi:10.1016/j.jssc.2009.07.046

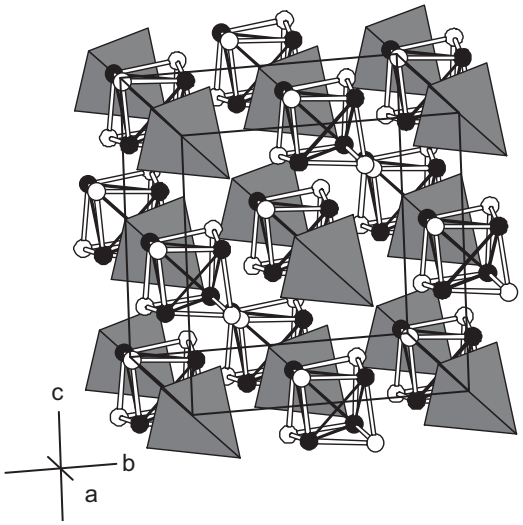

Fig. 1. The defect thiospinel structure of AB_4S_8. *B* atoms are shown as solid circles, sulfur by open circles and AS_4 tetrahedra are shaded. *B*–*S* bonds are shown as open lines and solid lines denote the *B*–*B* interactions that define a B_4 cluster.

In the same work, we also demonstrated that *B*-site substitution in $GaV_{4-x}Mo_xS_8$ suppresses both the structural distortion and the magnetic ordering transition.

While GaV_4S_8, with one unpaired electron per V_4 cluster, is ferromagnetic ($T_C = 10$ K), GeV_4S_8, which contains two unpaired electrons per cluster is antiferromagnetic ($T_N = 13$ K) [7]. Chudo et al. [17] have shown that on cooling, GeV_4S_8 undergoes a structural transition from cubic to rhombohedral symmetry at 33 K, before becoming orthorhombic below the Néel temperature, whereas Bichler et al. have suggested the transition is directly from the cubic to orthorhombic phase [18]. The antiferromagnetic spin structure of GeV_4S_8 has recently been determined by powder neutron diffraction [19] and is described in the magnetic space group P_bmn2_1 with a magnetic propagation vector, $\mathbf{k} = (\frac{1}{2}, \frac{1}{2}, 0)$.

In an effort to explore the influence of the cluster electron count on the transport and magnetic properties of defect thiospinels, we have prepared a new series of non-stoichiometric phases $Ga_{1-x}Ge_xV_4S_8$ in which gallium is progressively replaced by germanium. Structural data reveal a solid solution is formed throughout the composition range $0 \le x \le 1$. However, both transport and magnetic properties show a remarkable dependence on the *A*-site composition.

2. Experimental

A series of materials of nominal composition, $Ga_{1-x}Ge_xV_4S_8$ ($0 \le x \le 1$), was prepared by high-temperature reaction. Stoichiometric quantities of high-purity germanium (Aldrich, 99.99%), vanadium (Alfa Aesar, 99.5%) and sulfur (Sigma Aldrich, 99.99%) powders were ground in an agate mortar and appropriate quantities of gallium (Alfa Aesar, 99.99%) pieces cut from an ingot were added to each reaction mixture. The mixtures were loaded into silica tubes and sealed under vacuum ($<10^{-4}$ Torr). For the preparation of quaternary phases, reaction mixtures were fired for 24 h at 600 °C and reground prior to firing for a further 2 days at the same temperature. An analogous procedure was used for the synthesis of the ternary compounds, with the reaction temperature being raised to 730 and 750 °C for GeV_4S_8 and GaV_4S_8 respectively. In all cases the reaction mixtures were placed directly into a furnace held at the appropriate temperature. At the completion of the heating period, products were cooled to room temperature at the natural rate (ca. 5 °C min^{-1}) of the furnace. Reaction progress was monitored by powder X-ray diffraction, performed using a Bruker D8 Advance powder diffractometer operating with germanium-monochromated Cu$K\alpha_1$ radiation ($\lambda = 1.5405$ Å) and fitted with a Bruker LynxEye^{TM} linear detector. Data were collected over the angular range $10 \le 2\theta/^\circ \le 120$ in 0.014° angular increments, counting for 2.4 s at each detector position. Powder neutron diffraction data were collected at room temperature on the D2B diffractometer ($\lambda = 1.59379$ Å) at ILL, Grenoble. Samples (ca. 3 g) were contained in a vanadium can and patterns over the angular range $10 \le 2\theta/^\circ \le 160$ were recorded over a period of ca. 6 h. Rietveld analysis of powder diffraction data was undertaken using the GSAS [20] suite of programs. Sulfur contents were determined thermogravimetrically by oxidation in a flow of oxygen on a DuPont Instruments 951 Thermogravimetric Analyzer.

The electrical resistance of the samples over the temperature range $77 \le T/K \le 300$ was determined using a four-probe DC technique. An ingot (ca. $6 \times 3 \times 1$ mm) was cut from a sintered pellet and four 50 μm silver wires were attached, using colloidal silver paint, to provide connections to an HP34401A multimeter. The sample was placed in an Oxford Instruments CF1200 cryostat connected to an ITC502 temperature controller.

Measurements of the Seebeck coefficient over the temperature range $100 \le T/K \le 300$ were made on an ingot (ca. $8 \times 4 \times 1$ mm) also cut from a sintered pellet. This was then mounted on a copper holder using Apiezon® Type N grease. The copper holder incorporates a small heater (120 Ω strain gauge) located close to one end of the sample and is attached to the hot stage of a closed-cycle refrigerator (DE-202, Advanced Research Systems), controlled by a Lakeshore LS-331 temperature controller. Two 50 μm copper wires were attached to the ends of the sample using silver paint and connections made to a Keithley 2182A nanovoltmeter. Two Au: 0.07% Fe vs. chromel thermocouples were placed close to the sample at the hot and cold ends, and connected to a second Lakeshore LS-331 temperature controller. The Seebeck coefficient at a given temperature was determined by applying a temperature gradient, ΔT, across the sample and measuring the corresponding thermal voltage, ΔV. The slope of the line, $\Delta V/\Delta T$, was used to determine the Seebeck coefficient. The data were corrected for contributions due to the copper wires.

The magnetic properties of the samples over the temperature range $5 \le T/K \le 310$ were measured using a Quantum Design MPMS2 SQUID magnetometer. Samples were loaded into gelatin capsules at room temperature. Data were collected both after cooling in zero applied field (zfc) and after cooling in the measuring field (fc) of 1000 G. Data were corrected for the diamagnetism of the gelatine capsule and for intrinsic core diamagnetism.

3. Results

Powder X-ray diffraction data throughout the composition range $0 \le x \le 1$ can be indexed on the basis of a face-centered cubic unit cell. The initial structural model, for Rietveld refinement of the structure of the end-member phase GaV_4S_8, was that of Pocha et al. [16], described in the space group $F\bar{4}3m$, whilst for GeV_4S_8 the atomic coordinates of Johrendt [7] were used for the initial structural model. The structural model for the quaternary phases was obtained from that for GaV_4S_8 by progressively introducing germanium in place of gallium at the *A*-cation site. The refined lattice parameters of the end-member phases are in excellent agreement with those reported previously [7,16], while the compositional variation of the lattice parameters, obtained from Rietveld refinement using powder X-ray diffraction data, reveal (Fig. 2) that the unit-cell volume decreases with increasing levels

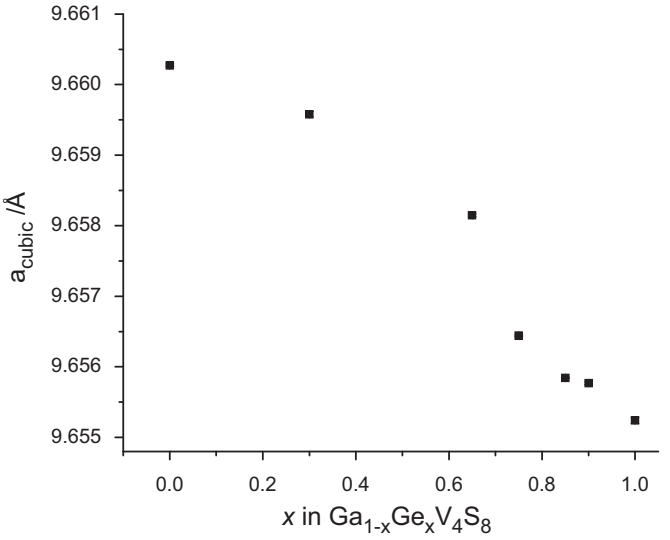

Fig. 2. Compositional dependence of the cubic unit cell parameter of $Ga_{1-x}Ge_xV_4S_{8-\delta}$ ($0 \le x \le 1$) determined by powder X-ray diffraction. Error bars lie within the points.

of germanium substitution. Given the similar atomic numbers of gallium and germanium, for a subset of quaternary phases, refinement of the structural model was carried out against powder X-ray and neutron diffraction data simultaneously, in order to confirm that germanium is incorporated in a disordered fashion exclusively at the *A*-cation (4(a)) site, initially occupied by gallium alone.

Weak reflections are observed in the neutron data in the regions, $d = 2.1$–2.2, 1.5–1.6 and 1.2–1.3 Å, originating from the vanadium sample can ($d_{110} = 2.14$ Å, $d_{200} = 1.52$ Å and $d_{211} = 1.24$ Å). Given the extremely low intensity of these reflections, it was not found necessary to exclude them from the refinements. The background of the neutron data was modeled using a cosine Fourier series whilst a linear interpolation function was used to fit the background of the X-ray data. Following initial refinement of scale factors, background terms, X-ray zero-point, positional, lattice parameters and thermal parameters were introduced as variables into the refinement. In all cases, the thermal parameters for Ga and Ge were constrained to be equal and also a single thermal parameter was used for both the vanadium and sulfide ions. A pseudo-Voigt peak shape was used for both X-ray and neutron data, with the coefficients introduced as refinable parameters. Site occupancy factors of gallium and germanium were allowed to vary with the constraint that the overall stoichiometry was maintained. The refined site occupancy factors result in a Ga:Ge ratio in excellent agreement with the nominal composition of the initial reaction mixture. The final cycles of refinement produced residuals in the range 4.58–5.12% (X-ray) and 3.25–4.81% (neutron). The remaining contribution to the weighted residuals in the X-ray data is principally associated with difficulties in describing the peak shape using the functions implemented in GSAS. However, values of $\chi^2 \approx 2$, provide a high degree of confidence in the correctness of the refined structural model. Representative observed, calculated and difference profiles from the simultaneous X-ray/neutron refinement are presented in Fig. 3. Corresponding profiles for the remaining compositions, together with those obtained using X-ray diffraction data alone are provided as supplementary information. Refined structural parameters for the subset of materials for which structural refinement was carried out against X-ray and neutron diffraction data simultaneously are presented in Table 1, whilst those for a wider range of compositions, obtained from X-ray diffraction data

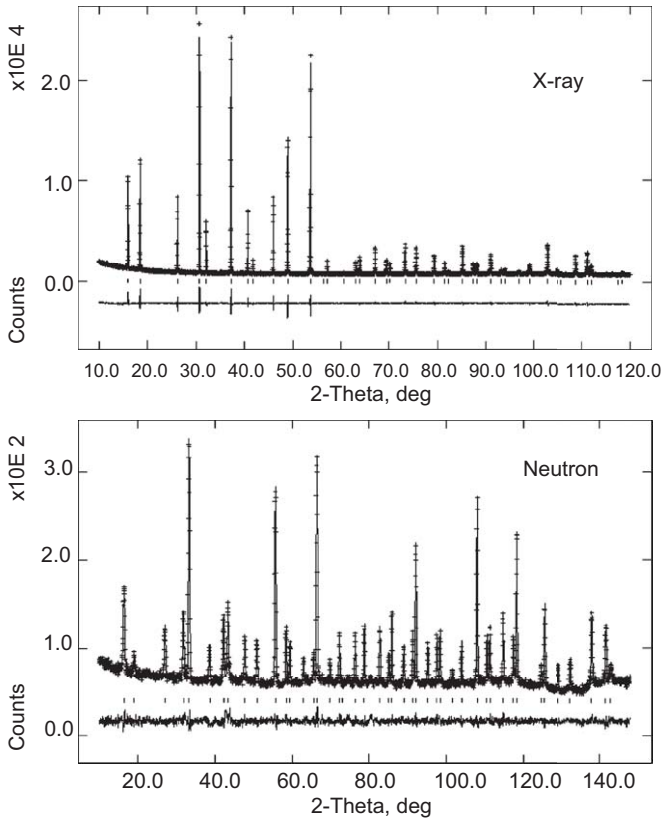

Fig. 3. Final, observed (crosses), calculated (upper full line) and difference (lower full line) powder diffraction profiles for the phase of nominal composition $Ga_{0.35}Ge_{0.65}V_4S_8$ at 298 K, Upper plot: X-ray data; Lower plot: neutron data. Reflection positions are marked.

alone, are provided as supplementary information. Selected bond distances and angles are presented in Table 2.

Thermogravimetric data are provided as supplementary information and summarized in Table 3. For all compositions, an initial weight loss at ca. 400 °C is followed by a small weight gain at ca. 670 °C. The weight loss step occurs at a higher temperature for the quaternary phases than for either of the end-member phases. Powder X-ray diffraction data for the products of thermogravimetric analysis demonstrate that the initial weight loss is caused by conversion of the ternary sulfide to a mixture of V_6O_{13}, Ga_2O_3 and/or GeO_2. However, depending on the point at which the TGA experiment is halted following this initial weight loss, small but varying amounts of V_2O_5 are also present. This introduces an uncertainty into the sulfur contents determined from this weight change and the values obtained (which indicate sulfur deficiencies between 2.8% and 7.5%) represent lower limits for the sulfur content. The subsequent weight gain is due to the oxidation of V_6O_{13} to V_2O_5. Therefore, the overall weight change for the conversion of the mixed-metal sulfide to a mixture of V_2O_5, Ga_2O_3 and/or GeO_2 was used to determine the sulfur contents shown in Table 3. The thermogravimetric data suggest that the end-member phases are essentially fully stoichiometric in sulfur but as the series is traversed, intermediate compositions show a sulfur deficiency of up to 2.9%, suggesting the formulation $Ga_{1-x}Ge_xV_4S_{8-\delta}$ ($0 \le \delta \le 0.23$). Attempts to locate the sulfur vacancies by Rietveld analysis were unsuccessful. This is due to the small change in scattering power at the 16(*e*) sites that such a defect concentration would create, together with correlation between site occupancy factors and thermal parameters and the disordering of sulfur vacancies over the available sites. The sulfur deficiency affects the number of electrons available to the cluster,

Table 1
Final refined parameters for $Ga_{1-x}Ge_xV_4S_8$ ($0<x<1.0$) described in the space group $F\bar{4}3m$[a], determined from refinement against powder X-ray and neutron diffraction data simultaneously.

x in $Ga_{1-x}Ge_xV_4S_8$	0.9	0.85	0.75	0.65	0.3
T (K)	298	298	200	298	298
a (Å)	9.65550(2)	9.65565(1)	9.65640(1)	9.65803(1)	9.65958(2)
A					
SOF(Ga)	0.08(5)	0.18(5)	0.31(3)	0.39(3)	0.66(4)
SOF(Ge)	0.92(5)	0.82(5)	0.69(3)	0.61(3)	0.34(4)
B (Å^2)	0.41(3)	0.18(3)	0.32(2)	0.47(2)	0.38(3)
V					
B (Å^2)	0.49(1)	0.34(1)	0.44(1)	0.50(1)	0.40(1)
x	0.60414(5)	0.60439(5)	0.60435(6)	0.60466(5)	0.60533(5)
S(1)					
B (Å^2)	0.49(1)	0.34(1)	0.44(1)	0.50(1)	0.40(1)
x	0.36988(8)	0.36916(8)	0.37086(8)	0.37089(7)	0.37125(8)
S(2)					
B (Å^2)	0.49(1)	0.34(1)	0.44(1)	0.50(1)	0.40(1)
x	0.86518(8)	0.86545(8)	0.86452(8)	0.86437(7)	0.86392(9)
R_{wp} (%) (neutron)	4.63	3.25	4.81	3.81	3.59
R_{wp} (%) (X-ray)	4.97	4.58	4.64	5.12	4.67
χ^2	2.11	1.79	2.28	2.33	1.80

[a] A on 4(a) (0,0,0); V, S(1) and S(2) on 16(e) (x,x,x).

Table 2
Bond distances (Å) and bond angles (deg) for $Ga_{1-x}Ge_xV_4S_8$ ($0\le x\le 1$) obtained from Rietveld refinement against powder diffraction data collected at 298 K.

x in $Ga_{1-x}Ge_xV_4S_8$	1.0[a]	0.9[b]	0.85[b]	0.75[a]	0.65[b]	0.3[b]	0.0[a]
A–S(2)	4 × 2.2543(23)	4 × 2.255(1)	4 × 2.250(1)	4 × 2.2743(13)	4 × 2.269(1)	4 × 2.277(1)	4 × 2.2657(18)
V–S(1)	3 × 2.2789(18)	3 × 2.290(1)	3 × 2.300(1)	3 × 2.2745(10)	3 × 2.282(1)	3 × 2.284(1)	3 × 2.3040(14)
V–S(2)	3 × 2.5603(15)	3 × 2.555(1)	3 × 2.554(1)	3 × 2.5437(8)	3 × 2.544(1)	3 × 2.533(1)	3 × 2.5299(11)
Intracluster V–V distances	3 × 2.8318(26)	3 × 2.844(2)	3 × 2.851(1)	3 × 2.8517(14)	3 × 2.859(2)	3 × 2.878(2)	3 × 2.8970(19)
Intercluster V–V distances	3 × 3.9954(26)	3 × 3.983(2)	3 × 3.977(1)	3 × 3.9765(14)	3 × 3.970(2)	3 × 3.952(2)	3 × 3.9339(19)
S(2)–A–S(2)	6 × 109.471(−)	6 × 109.471(−)	6 × 109.471(−)	6 × 109.471(−)	6 × 109.471(−)	6 × 109.471(−)	6 × 109.471(−)
S(1)–V–S(1)	3 × 101.77(7)	3 × 102.1(4)	3 × 101.8(5)	3 × 101.12(4)	3 × 101.19(4)	3 × 100.74(4)	3 × 100.91(5)
S(1)–V–S(2)	6 × 89.73(6)	6 × 89.54(3)	6 × 89.45(3)	6 × 90.280(31)	6 × 90.12(3)	6 × 90.39(3)	6 × 90.02(4)
S(2)–V–S(2)	3 × 75.81(8)	3 × 75.98(5)	3 × 76.23(4)	3 × 75.49(5)	3 × 75.77(4)	3 × 75.82(5)	3 × 76.46(6)

[a] Refinement carried out against powder X-ray diffraction data.
[b] Refinement carried out against powder X-ray and neutron diffraction data simultaneously.

Table 3
Results of thermogravimetric analysis of $Ga_{1-x}Ge_xV_4S_{8-\delta}$ ($0\le x\le 1$) phases.

Nominal composition	GaV_4S_8	$Ga_{0.9}Ge_{0.1}V_4S_8$	$Ga_{0.75}Ge_{0.25}V_4S_8$	$Ga_{0.7}Ge_{0.3}V_4S_8$	$Ga_{0.5}Ge_{0.5}V_4S_8$	$Ga_{0.45}Ge_{0.55}V_4S_8$
Overall weight change (%)	−13.6	−13.28	−13.7	−12.72	−12.17	−11.64
Experimentally determined composition[a]	$GaV_4S_{7.99(4)}$	$Ga_{0.9}Ge_{0.1}V_4S_{7.95(4)}$	$Ga_{0.75}Ge_{0.25}V_4S_{8.07(5)}$	$Ga_{0.7}Ge_{0.3}V_4S_{7.91(3)}$	$Ga_{0.5}Ge_{0.5}V_4S_{7.86(4)}$	$Ga_{0.45}$-$Ge_{0.55}V_4S_{7.77(3)}$
Nominal number of d-electrons per V_4 cluster	7	7.1	7.25	7.3	7.5	7.55
Number of d-electrons per V_4 cluster[b]	7.03	7.19	7.08	7.48	7.77	8.00
Nominal composition	$Ga_{0.4}Ge_{0.6}V_4S_8$	$Ga_{0.35}Ge_{0.65}V_4S_8$	$Ga_{0.3}Ge_{0.7}V_4S_8$	$Ga_{0.25}Ge_{0.75}V_4S_8$	$Ga_{0.1}Ge_{0.9}V_4S_8$	GeV_4S_8
Overall weight change (%)	−11.85	−11.51	−12.1	−11.71	−12.14	−11.62
Experimentally determined composition[a]	$Ga_{0.4}Ge_{0.6}V_4S_{7.84(2)}$	$Ga_{0.35}Ge_{0.65}V_4S_{7.79(6)}$	$Ga_{0.3}Ge_{0.7}V_4S_{7.91(4)}$	$Ga_{0.25}Ge_{0.75}V_4S_{7.85(4)}$	$Ga_{0.1}Ge_{0.9}V_4S_{7.98(2)}$	$GeV_4S_{7.91(4)}$
Nominal number of d-electrons per V_4 cluster	7.6	7.65	7.7	7.75	7.9	8
Number of d-electrons per V_4 cluster[b]	7.92	8.08	7.88	8.04	7.94	8.18

[a] Normalized to a Ga/Ge content of 1 mol/formula unit.
[b] For experimentally determined composition.

which towards the middle of the series deviates from that expected from the nominal stoichiometries (Table 3). In particular, on germanium substitution, the number of cluster electrons reaches the 8 e^-/cluster expected for complete substitution at ca. 55% germanium incorporation.

Zero-field-cooled and field-cooled magnetic susceptibility data for all materials (Fig. 4) overlie each other over the entire temperature range studied. The end-member phase $GeV_4S_{8-\delta}$ exhibits modified Curie–Weiss behavior, with a temperature-independent contribution to the susceptibility comparable to that

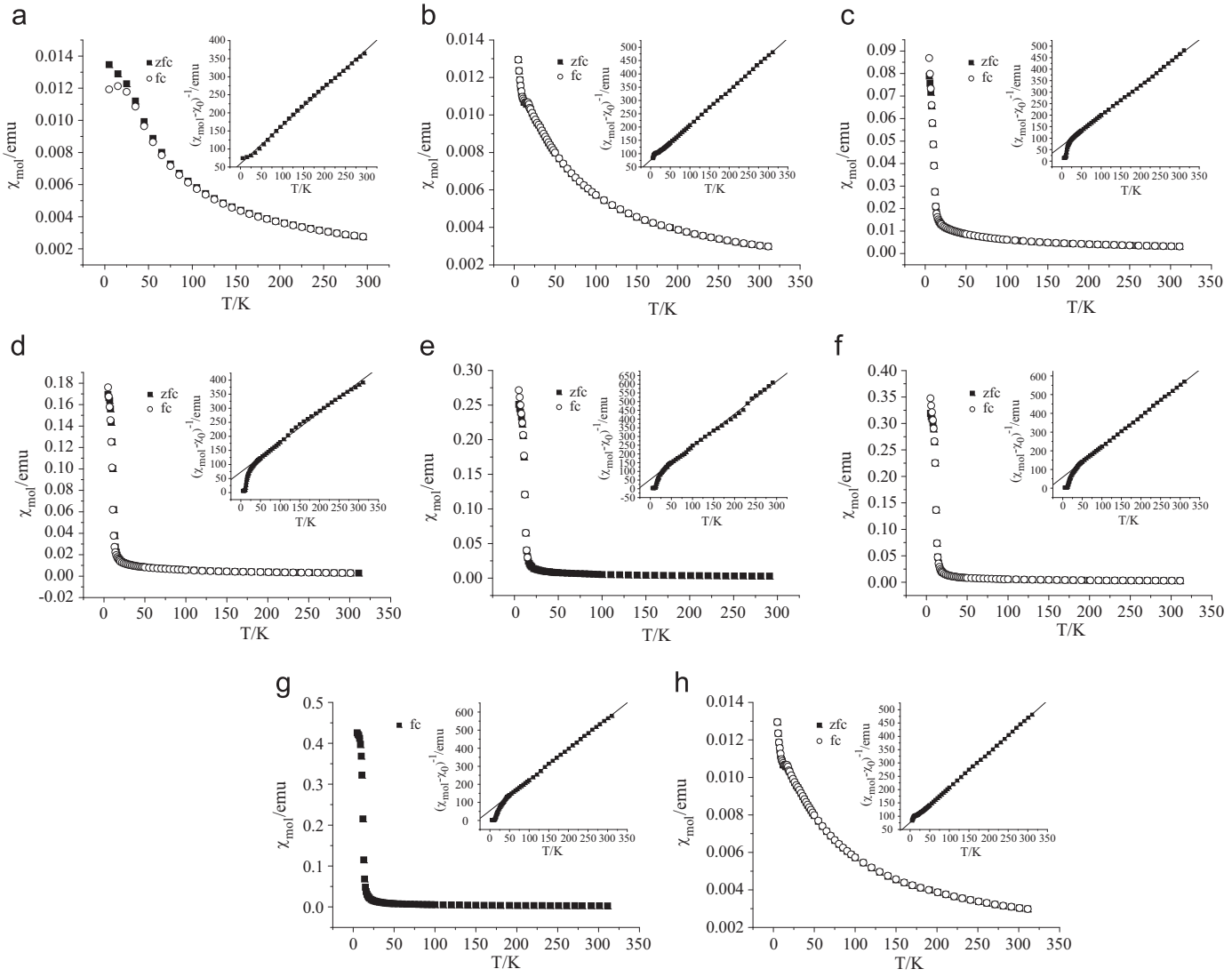

Fig. 4. Zero-field-cooled (zfc) and field-cooled (fc) molar magnetic susceptibility data for $Ga_{1-x}Ge_xV_4S_{8-\delta}$: (a) $x = 1$, (b) $x = 0.75$, (c) $x = 0.7$, (d) $x = 0.65$, (e) $x = 0.6$, (f) $x = 0.55$, (g) $x = 0.5$ (fc) data, (h) $x = 0.25$. Insets show reciprocal susceptibility data, with the solid line denoting the fit to a modified Curie–Weiss expression incorporating a temperature independent term, χ_0.

in the gallium analogue [13,16]. Data for the mixed $Ga_{1-x}Ge_xV_4S_{8-\delta}$ ($0<x\leq1$) phases were also fitted using a modified Curie–Weiss expression, incorporating a temperature-independent term, over a wide range of temperatures, with deviations being observed only at low temperatures. Magnetic parameters derived from the fits to reciprocal susceptibility data are presented in Table 4. All phases exhibit a significant temperature-independent contribution, χ_0, to the susceptibility, values of χ_0 being generally higher for the quaternary phases than for the end members. The effective magnetic moment, μ_{eff}, of $GaV_4S_{8-\delta}$ is ca. 1.6 μ_B per vanadium–sulfur cluster. This is close to the value for a single unpaired electron, which the molecular orbital treatment of Pocha et al. [16] predicts for $V_4S_4^{5+}$. Substitution of Ga^{3+} with Ge^{4+} causes reduction of the cluster which would be expected to increase μ_{eff}. The increase in measured moment compares favorably with the spin-only value predicted on the basis of the changing occupation of the cluster orbitals. (Fig. 5). The observation of negative Weiss constants for all non-stoichiometric materials suggests that the dominant exchange interactions are antiferromagnetic in origin.

For all samples with $x\leq0.7$, the reciprocal susceptibility data exhibit a discontinuity around 40 K that comparison with the end-member $x = 0$ phase [16] suggests is due to a structural distortion. The second lower temperature anomaly in $\chi^{-1}(T)$, which corresponds to a marked increase in magnetization, indicates that the ferromagnetic behavior of $GaV_4S_{8-\delta}$ is retained to $x\leq0.7$, with $T_C\approx20$ K. The magnitude of the low temperature susceptibility of the materials decreases with increasing germanium content, until at compositions with $x>0.7$, the low-temperature magnetization is greatly reduced and a local maximum is introduced into $\chi(T)$. It would thus appear that $Ga_{0.25}Ge_{0.75}V_4S_{8-\delta}$ exhibits antiferromagnetic order, similar to that of the end-member $x = 1$ phase, with $T_N = 15$ K.

The end-member phases, $GaV_4S_{8-\delta}$ and $GeV_4S_{8-\delta}$, exhibit semiconducting behavior (Fig. 6). The mechanism of the conductivity in nominally stoichiometric GaV_4S_8 was investigated in detail by Sahoo and Rastogi [14] who reported that the activation energy varies from 0.14 eV at room temperature to 0.04 eV at 80 K. It was proposed that this reduction is the result of multi-electron hopping of carriers. By fitting the linear portion of the $\ln(\rho)$ vs. $1/T$ curve (Supporting Information), an activation energy of 0.08(2) eV, is obtained, which is within the range previously reported. The analogous plot for $GeV_4S_{8-\delta}$ is non-linear, indicating that it does not exhibit simple thermally

Table 4
Magnetic properties of $Ga_{1-x}Ge_xV_4S_{8-\delta}$ ($0 \le x \le 1$) phases derived from fits to a modified Curie–Weiss expression.

x in $Ga_{1-x}Ge_xV_4S_{8-\delta}$	Data range (K)	C ($cm^3\,K\,mol^{-1}$)	θ (K)	χ_0 ($10^{-4}\,cm^3\,mol^{-1}$)	μ_{eff} per V_4 cluster
0.0 [13]	45–295	0.304(3)	−12.4(6)	4.3(1)	1.559(8)
0.25	50–310	0.397(5)	−18.9(7))	11.0(2)	1.78(1)
0.50	40–310	0.58(2)	−31(2)	8.7(5)	2.15(4)
0.55	40–310	0.612(9)	−36(1)	10.8(3)	2.21(1)
0.60	40–310	0.61(3)	−40(3)	12.0(1)	2.21(5)
0.65	40–310	0.77(2)	−48(2)	3.2(6)	2.48(3)
0.70	40–300	0.747(7)	−50(7)	11.0(2)	2.44(2)
0.75	40–300	0.765(6)	−58.3(6)	9.0(5)	2.47(1)
1.0	35–295	0.737(7)	−33.6(6)	5.0(2)	2.43(1)

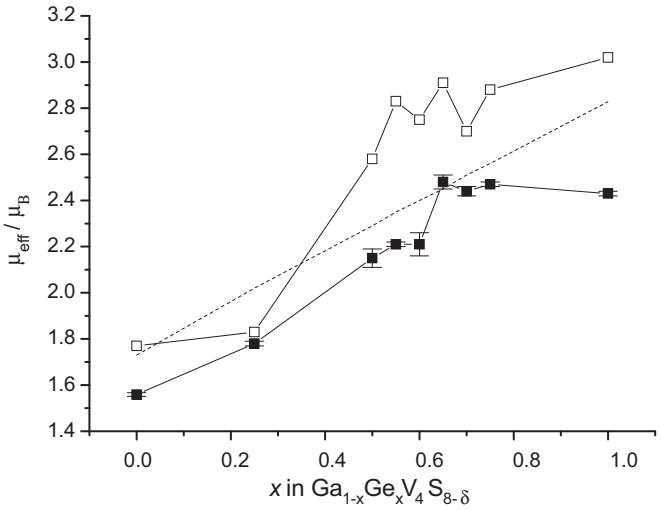

Fig. 5. Comparison of effective magnetic moments (solid points), determined from a fit to a modified Curie–Weiss expression, with the spin-only values calculated for the analytically determined composition (open points). The dashed line represents the variation in spin-only values expected for progressive replacement of Ga by Ge in materials fully stoichiometric in sulfur.

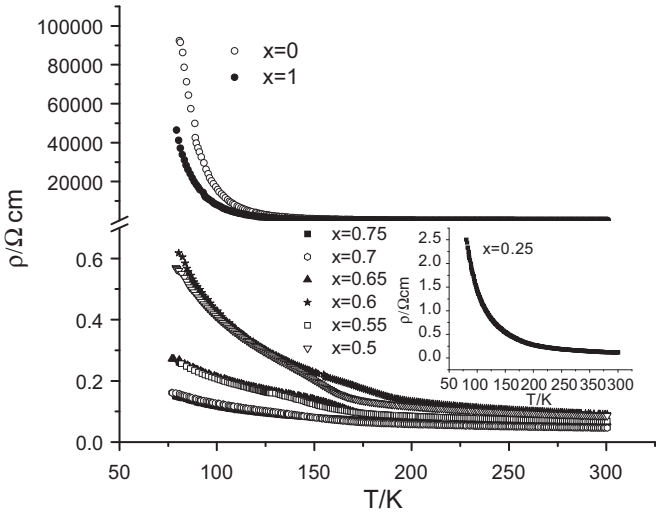

Fig. 6. Electrical transport property data for $Ga_{1-x}Ge_xV_4S_{8-\delta}$ ($0 \le x \le 1$).

activated conduction. However $\ln(\rho/T^{1/2})$ shows a linear dependence on $T^{-1/4}$ (Supporting Information) consistent with a variable-range hopping conduction mechanism of the form [21]

$$\rho = \rho_0 \left(\frac{T}{T_0}\right)^{1/2} \exp\left[\left(\frac{T_0}{T}\right)^{v}\right]$$

with the exponent $v = \frac{1}{4}$ indicating a three-dimensional conduction mechanism.

The temperature dependence of the electrical resistivity of all quaternary phases (Fig. 6) also indicates semiconducting behavior. However, there is a significant reduction of the resistivity relative to that of either of the end-member phases. For materials containing both gallium and germanium, the magnitude of the resistivity decreases with increasing germanium content such that $Ga_{0.25}Ge_{0.75}V_4S_{8-\delta}$, despite remaining semiconducting throughout the temperature range investigated, exhibits a resistivity at low temperature (ca. 80 K) that is almost six orders of magnitude lower than that of $GaV_4S_{8-\delta}$. The conduction mechanism for the quaternary phases also appears to be of the variable-range hopping type (Supporting Information) as observed in the end-member phase $GeV_4S_{8-\delta}$. This suggests that the conduction in materials in the range ($0 < x \le 1$) is dominated by hopping of charge carriers between states localized on opposite sides of the Fermi energy. Furthermore, with the exception of the material $Ga_{0.75}Ge_{0.25}V_4S_{8-\delta}$, a resistivity anomaly not present in the end members is observed in the region 140–180 K. The origin of this anomaly is unclear. Johrendt has suggested [7] that the electronic structure of ordered-defect thiospinels is extremely sensitive to subtle structural distortions of the V_4 cluster from tetrahedral symmetry. Our own preliminary analysis of neutron diffraction data provide no evidence for a reduction from cubic symmetry at 180 K. However, investigation of subtle structural changes involving distortion of the vanadium sub-lattice in this region of temperature, would reqire the use of high-resolution X-ray diffraction data.

The large negative Seebeck coefficient of $GaV_4S_{8-\delta}$ (Fig. 7) indicates that the dominant charge carriers are electrons. Although the plots presented by Sahoo and Rastogi [14] for nominally stoichiometric GaV_4S_8 appear to indicate p-type behavior, they state clearly in the text that it is an n-type semiconductor, in agreement with the data presented here. They have shown, however, that the Seebeck coefficient of GaV_4S_8 is dependent both on sample preparation and gallium content. Quenching the sample significantly changes the values of Seebeck coefficient and 33% gallium excess results in a change of sign at low temperatures. The other end-member phase $GeV_4S_{8-\delta}$ exhibits hole-type conduction as evidenced by the positive Seebeck coefficient (Fig. 7), although its absolute value is significantly lower than that of $GaV_4S_{8-\delta}$. For the quaternary phases reported here, the Seebeck coefficient in the temperature

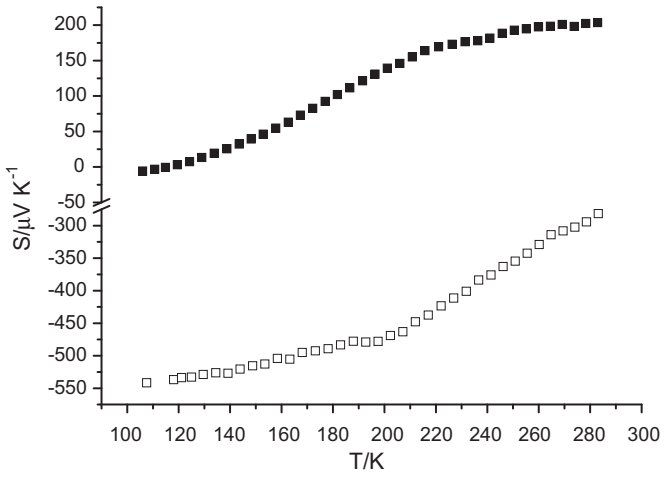

Fig. 7. Seebeck coefficient data for $GaV_4S_{8-\delta}$ (open points) and $GeV_4S_{8-\delta}$ (solid points) collected over the temperature range $100 \leq T/K \leq 300$.

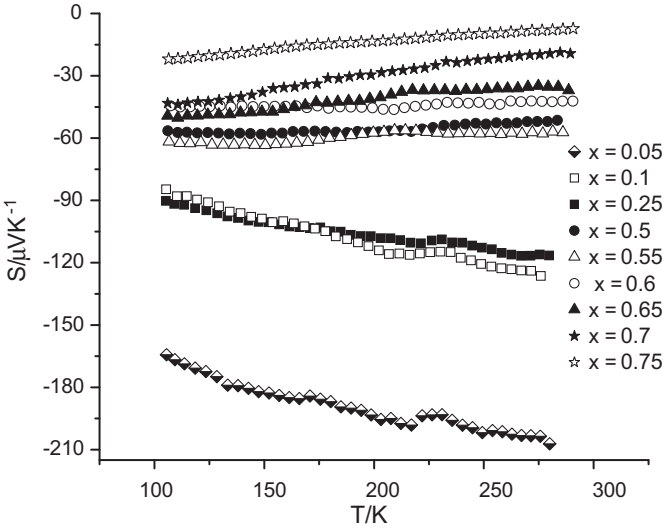

Fig. 8. Seebeck coefficient data for quaternary phases $Ga_{1-x}Ge_xV_4S_{8-\delta}$ $(0<x<1)$ collected over the temperature range $100 \leq T/K \leq 300$.

range $100 \leq T/K \leq 300$ is negative (Fig. 8) and shows a much weaker dependence on temperature than that of either of the end members. At a given temperature, the absolute value of the Seebeck coefficient decreases with increasing germanium content (Fig. 9), which correlates with the marked reduction in resistivity with increasing levels of substitution.

4. Discussion

Structural refinement using a combination of powder X-ray and neutron diffraction confirms that germanium is incorporated in $Ga_{1-x}Ge_xV_4S_{8-\delta}$ exclusively at the tetrahedral 4(a) site, where it replaces gallium. This results in a reduction in the unit cell volume, consistent with the smaller ionic radius [22] of Ge^{4+} (0.39 Å) compared with Ga^{3+} (0.47 Å).

The intracluster V–V distance of 2.832(3) Å for $GeV_4S_{8-\delta}$ is somewhat shorter than that of the gallium analogue (2.897(2) Å). This reduction may be associated with the increased population of bonding states in the former. This view is supported by the further shortening of the intracluster cation–cation distance to 2.814(3) Å

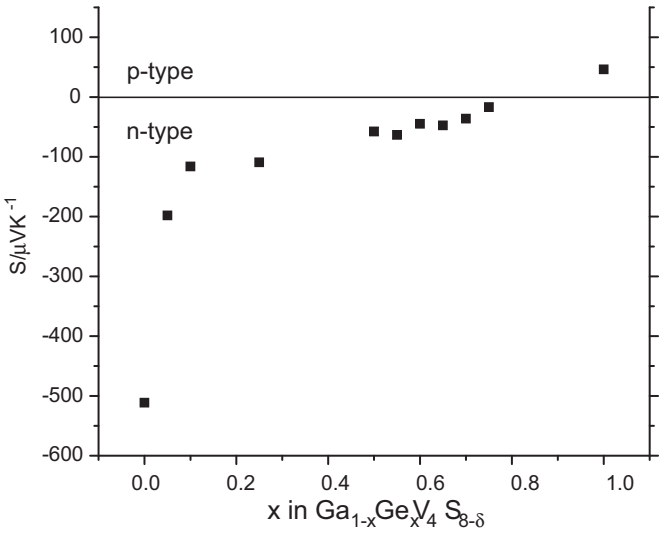

Fig. 9. The compositional variation of the Seebeck coefficient of $Ga_{1-x}Ge_xV_4S_{8-\delta}$, $(0 \leq x \leq 1)$ at 215 K.

in the related phase $GaMo_4S_8$, in which there are 11 bonding electrons associated with the Mo_4S_4 cluster [16]. In the $Ga_{1-x}Ge_xV_4S_{8-\delta}$ phases reported here, the reduction of the intracluster V–V distance with increasing levels of germanium substitution (Fig. 10) may thus be related to the increasing electron population of bonding states. This shortening of the intracluster V–V distance, together with a corresponding increase in the intercluster V–V separation (Fig. 10), suggests that the deviation from the ideal spinel structure increases with increasing substitution at the *A*-site. This may be quantified [23] through the degree of clustering of the *B*-site cations ($D^{BB} = [(d_{B\ldots B}/d_{B-B})-1] \times 100\%$, where $d_{B\ldots B}$ and d_{B-B} denote, respectively, intercluster and intracluster *B*–*B* distances) and the degree of distortion of the transition-metal coordination from the ideal octahedral geometry ($D^{BS} = [(d_{B-S2}/d_{B-S1})-1] \times 100\%$). Both of these parameters correlate with the cluster electron count, corrected for the effects of sulfur deficiency (Fig. 11). Both the degree of clustering and the distortion from octahedral symmetry increase with increasing electron count. This is consistent with the increased population, on traversing the $Ga_{1-x}Ge_xV_4S_{8-\delta}$ series, of levels which molecular orbital calculations indicate have strong *B*–*B* bonding character. Similarly it has been shown [9] that depopulation of these levels in $Ga_{0.87}Ti_4S_8$ (ca. 3 e^- per cluster) leads to partial de-clustering as evidenced by longer *B*–*B* distances and less distortion of the local coordination around *B*.

It has been proposed [9] that partial de-clustering of the Ti_4S_4 cluster in $Ga_{0.87}Ti_4S_8$ is responsible for the metallic behavior of this phase as a result of the strengthening of inter-cluster transfer integrals. This would suggest that the increased clustering with increasing germanium content that occurs in the $Ga_{1-x}Ge_xV_4S_{8-\delta}$ series of phases reported here would weaken the transfer integrals, resulting in a decrease in electron mobility. However, both the resistivity and Seebeck data are consistent with the non-stoichiometric materials being more conductive than either of the end-member phases, although the materials remain semiconducting throughout the composition range and values of μ_{eff} indicate that localized electron behavior is retained. This suggests that the changes in the electron transport properties of $Ga_{1-x}Ge_xV_4S_{8-\delta}$ are associated with a change in charge carrier density rather than electron mobility.

Formal valence considerations suggest that the positive charge on the V_4S_4 cluster should reduce by one unit between $x = 0$ and 1 in the series $Ga_{1-x}Ge_xV_4S_8$. This would correspond to the addition

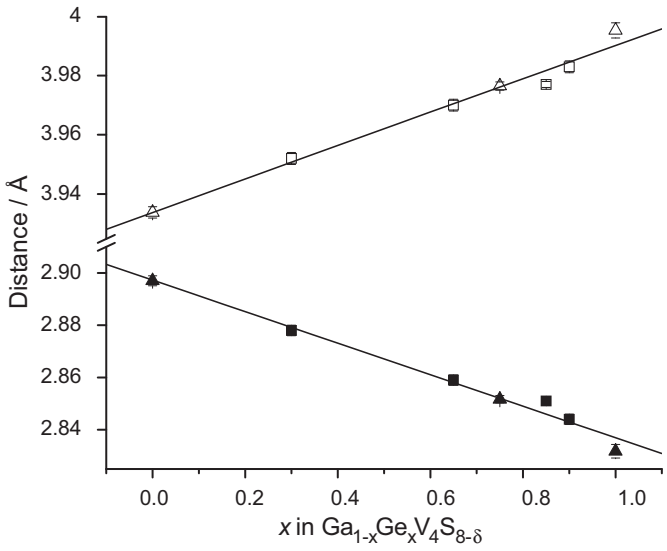

Fig. 10. Variation with composition of V–V distances of $Ga_{1-x}Ge_xV_4S_{8-\delta}$ phases at 298 K. Intra- and inter-cluster distances are denoted by solid and open points, respectively. Squares denote values were determined from Rietveld refinement using neutron and powder X-ray diffraction data simultaneously and triangles, values determined from powder X-ray diffraction data alone. The straight lines are a guide to the eye.

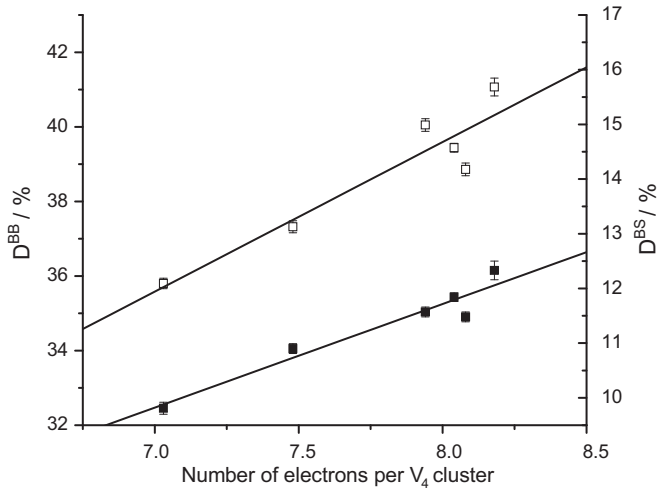

Fig. 11. Variation of the D^{BB} (open points) and D^{BS} (solid points) parameters with the number of $Ga_{1-x}Ge_xV_4S_{8-\delta}$. The number of electrons per metal cluster was calculated for experimentally determined compositions. The straight lines are a guide to the eye.

of one electron to the cluster orbitals on traversing the series. However, thermogravimetric analysis reveals that sulfur deficiency also plays a role, raising the electron count associated with the vanadium sulfur cluster for materials in the substitution range $0.3 \leq x \leq 0.75$ above that expected on the basis of nominal stoichiometries. The molecular orbital treatment of Pocha et al. [16] indicates that for the cubic phase, electrons are accommodated in orbitals (in ascending order of energy) of a_1, e and t_2 symmetry (Fig. 12). Therefore for all materials investigated in the present work, it is the population of the highest lying t_2 orbitals that changes with germanium substitution. Band structure calculations have been performed for the end-member phases GaV_4S_8 [16] and GeV_4S_8 [7]. In GeV_4S_8, states in the region of the Fermi level, E_F, are almost purely V–V bonding levels, with little dispersion and hence a narrow bandwidth. It has been suggested

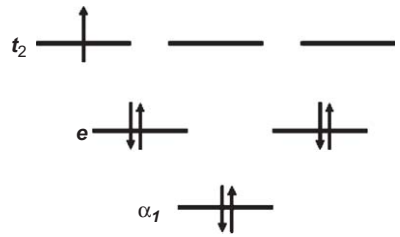

Fig. 12. Molecular orbital scheme of the B_4 cluster orbitals in AB_4S_8 (after Pocha et al. [16]). The orbital filling refers to the composition GaV_4S_8.

[7] that it is the narrowness of the bands relative to the on-site repulsion energy, U, that is responsible for the non-metallic character of GeV_4S_8, despite the absence of an energy gap at E_F. Similarly GaV_4S_8 exhibits a band of width ca. 0.7 eV at E_F. A general feature of these phases is therefore a highly structured density of states, with sharp peaks in the region of E_F. As the density of states changes rapidly with increasing energy, it suggests that the charge-carrier density at E_F is an extremely sensitive function of the degree of band filling. Therefore we suggest that the increased conductivity in the substituted phases reflects an increase in charge-carrier density. The decrease in the absolute value of the Seebeck coefficient with increasing levels of germanium incorporation suggests that hole conduction assumes greater significance as the degree of band filling increases, with the result that the conductivity-weighted sum of hole and electron contributions to the Seebeck coefficient that is measured becomes less negative. At full germanium substitution, the highest-lying t_2 band is over two-thirds full. The positive Seebeck coefficient of $GeV_4S_{8-\delta}$ suggests that holes in the spin-up band of the spin-polarized density of states dominate the conduction in this phase.

In conclusion, we have prepared a new series of defect thiospinels in which A-site substitution has been used to tune the electron count associated with the vanadium–sulfur cluster. However, sulfur vacancies in intermediate phases also play a role in determining the electron count. Whilst electrical transport properties reveal that semiconducting behavior is retained throughout the composition range, consistent with electron localization indicated by the magnetic data, the resistivity of the intermediate phases is markedly lower than that of either of the end-member phases. The results demonstrate that the electrical transport properties are a sensitive function of the electron count, which is consistent with previous suggestions that narrow band states arising from V–V interactions within the cluster principally determine the physical properties.

Supporting information

Observed, calculated and difference profiles from Rietveld analysis, thermal analysis data, additional electron-transport data and refined structural parameters for a wider range of compositions obtained from X-ray diffraction data alone can be found in the on-line version.

Acknowledgments

We wish to thank Heriot-Watt University for funding for I.S., whilst P.V. thanks the UK EPSRC for the award of an Advanced Research Fellowship.

Appendix A. Supplementary material

Supplementary data associated with this article can be found in the online version at doi:10.1016/j.jssc.2009.07.046.

References

[1] R.P. van Stapele, in: E.P. Wohlfarth (Ed.), Ferromagnetic Materials, vol. 3, North-Holland Publishing Company, 1982 (Chapter 8).
[2] A. Kjeshus, W.B. Pearson, Prog. Solid State Chem. 1 (1964) 83.
[3] P. Vaqueiro, A.V. Powell, Chem. Mater. 12 (2000) 2705.
[4] H. Barz, Mater. Res. Bull. 8 (1973) 983.
[5] C. Perrin, R. Chevrel, M. Sergent, C. R. Acad. Sci. Paris 280C (1975) 949.
[6] B. Yaich, J.C. Jegaden, M. Potel, M. Sergent, A.K. Rastogi, R. Tournier, J. Less Common Met. 102 (1984) 9.
[7] D. Johrendt, Z. Anorg. Allg. Chem. 624 (1998) 952.
[8] V.F. Shamrai, G.M. Leitus, Sov. Phys. Solid State 29 (1987) 1312.
[9] C. Vaju, J. Martial, E. Janod, B. Corraze, V. Fernandez, L. Cario, Chem. Mater. 20 (2008) 2382.
[10] Y. Sahoo, A.K. Rastogi, J. Phys. Chem. Solids 57 (1996) 467.
[11] C. Perrin, R. Chevrel, M. Sergent, J. Solid State Chem. 19 (1976) 305.
[12] D. Bichler, D. Johrendt, Chem. Mater. 19 (2007) 4316.
[13] A.V. Powell, A. McDowall, I. Szkoda, K.S. Knight, B.J. Kennedy, T. Vogt, Chem. Mater. 19 (2007) 5035.
[14] Y. Sahoo, A.K. Rastogi, J. Phys. Condens. Matter 5 (1993) 5953.
[15] A.K. Rastogi, A. Niazi, Physica B 223&224 (1996) 588.
[16] R. Pocha, D. Johrendt, R. Pöttgen, Chem. Mater. 12 (2000) 2882.
[17] H. Chudo, C. Michioka, H. Nakamura, K. Yoshimura, Physica B 378–380 (2006) 1150.
[18] D Bichler, V. Zinth, D. Johrendt, O. Heyer, M.K. Forthaus, T. Lorenz, M.M. Abd-Elmeguid, Phys. Rev. B 77 (2008) 212102.
[19] H. Müller, W. Kockelmann, D. Johrendt, Chem. Mater. 18 (2006) 2174.
[20] A.C. Larson, R.B. von Dreele, General Structure Analysis System, Los Alamos Laboratory, 1994 (Report LAUR 85-748).
[21] B.I. Shklovskii, A.L. Efros, Electronic Properties of Doped Semiconductors, Springer, Berlin, 1984.
[22] R.D. Shannon, Acta. Crystallogr. Sect. A 32 (1976) 751.
[23] R. Pocha, D. Johrendt, B. Ni, M.M. Abd-Elmeguid, J. Am. Chem. Soc. 127 (2005) 8732.